VOL. 21, NO. 8, APRIL 2026 ISSN 1819-6608
ARPN Journal of Engineering and Applied Sciences

www.arpnjournals.com

AN APPROACH FOR OPTIMUM FRACTURE DESIGN USING CENTRAL COMPOSITE DESIGN

Nguyen Huu Truong
Department of Petroleum Engineering, Petro Vietnam University, Vietnam
E-Mail: Truongnh@pvu.edu.vn

ABSTRACT

This study presents an approach to optimize the design of hydraulic fracture treatments in the low-permeability area of the Lower Miocene sandstone reservoir in the Cuu Long Basin of southern Vietnam. Six major design variables influenced the fracture length, which may enhance oil production when the fracture length was maximized. Thus, the fracture length was analyzed using the central composite face design based on statistical modeling, which is an experimental design for response surface methodology. The results showed that a maximum fracture length of 828 ft was obtained at an injection rate of 30 bpm with an injection time of 79 minutes. The slurry concentration at the end of the job was 8.6 ppg, the leak-off coefficient was 0.0023 ft/min$^{0.5}$, and the fracture height migration to the pay zone height ratio was 1.065.

Keywords: lower Miocene reservoir, optimum fracture geometry, central composite face-centered design, response surface methodology, design variables.

Manuscript Received 26 March 2026; Revised 13 April 2026; Published 20 June 2026

1. INTRODUCTION

Currently, hydraulic fracturing is a method of stimulating wells to improve oil and gas recovery from low permeability zones, and it has been widely utilized to enhance oil and gas extraction from low, moderate, and high-permeability reservoirs (Economides, Oligney, and Valko, 2002). This technique uses a pressurized fracturing fluid injection to create artificial fractures, which improve oil production by creating high permeability between the reservoir and the production wellbore (Rachmat, Pramana, and Febriana, 2012). Over the past few decades, several articles have presented and developed methods for hydraulic fracturing in sandstone reservoirs (Priyantoro *et al*., 2012; Bybee, 2003; Zhou *et al*., 2006; Roudakov & Rohwer, 2006; Zagrebelnyy *et al*., 2017). In general, the permeability of the Miocene reservoir in the White Tiger field varies and ranges from 2.8-2500 mD (Ngoc *et al*., 2013). When the permeability of the reservoir was low, between 0.1-10 mD, or moderate, between 5-50 mD, hydraulic fracturing could be applied to increase productivity (Holditch 1993; Economides *et al*. 2002). To extract large amounts of oil from the Lower Miocene reservoir, hydraulic fracturing has been used, and the fracture widths thereof have produced high fracture conductivity, which allows oil from the fractures to easily move to the wellbore. The input data of the fracture treatment design can be divided into two types of factors: uncontrolled and controlled. The controlled factors consist of fluid viscosity, the leak-off coefficient, the pump rate, the injection time, the proppant concentration at the end of the job, and the ratio of the fracture height migration to the pay zone height. The uncontrolled factors consist of in-situ stress, fracture toughness, Poisson's ratio, Young's modulus, and the fracture orientation of the formation properties, which were preferred in the Miocene reservoir of the White Tiger. The output parameters of the hydraulic fracture design include the determination of the fracture geometry, the evaluation of fracture conductivity, and a prediction of the post-fracture conductivity (Usman, Marino, Soelistijono 2010). Additionally, it is necessary to determine what proppant was used in the treatment, as the deciding proppant type, size, shape, mass, and concentration in the fractures (Van der Hoorn et al., 2012). (Meng and Brown, 1987); (Aggour and Economides, 1998), and (Langedijk *et al*., 2000) used a maximization of the net present value as the treatment design objective. The NPV is obtained from a sensitivity analysis considering the number of fracture treatments and the fracture length. (Mohaghegh *et al*., 1996) proposed a hybrid neuro-genetic algorithm for an optimal fracture treatment design based on recorded data. In addition, (Aggour, 2001) published a procedure for fracture treatment-design optimization in high-permeability reservoirs with an NPV objective using the gradient method to optimize the nonlinear issue. (Economides *et al*., 2002) presented a unified fracture design optimization based on the given proppant mass. Moreover, although their study was well conducted, it lacked the optimal surface parameters to maximize the fracture length. (Queipo *et al*., 2002) developed a method based on global optimization for hydraulic fracturing treatment design, which considered the Khristianovitch-Geertsma-de Klerk (KGD) (Valko and Economides, 1995) fracture model. However, their model is rarely used for stimulating oil and gas reservoirs and did not consider fluid viscosity as a free design variable. This study proposes a new method for predicting the optimum variable conditions using the central composite face design and response surface methodology for the maximum fracture length objective of hydraulic fracturing for the Lower Miocene sandstone

ISSN 1819-6608
ARPN Journal of Engineering and Applied Sciences

reservoir. The experimental design and response surface methodology are used to reduce risk and aim for optimal hydraulic fracturing conditions. There is a total of 47 tests based on one half of the fraction of the standard 2k factorial points for six variables in the experimental design. Each design has an injected volume to achieve the fracture length objective.

2. FRACTURE MODELS

In this research, the PKN-C fracture model of hydraulic fracturing in the Lower Miocene formation was designed based on the hydraulic fracturing program, namely Mfrac. This is a complete design and investigation of several output parameters through a simulator that contains a wide variety of options. Since 2018, Mfrac has been sponsored by Baker Hughes GE with licenses included. Several fracture models are available to define the fracture growth of the fracture geometry (length, height, and fracture width), which are functions of parameters based on the real models, such as 2D models (Perkins and Kern, 1961; Nordgren, 1972), pseudo-three-dimensional (p-3D) models (Rahim and Holditch, 1995), and three-dimensional (3D) models (Hossain, 2001). To estimate the exact fracture geometry during hydraulic fracturing in the Lower Miocene, a 2D fracture model, PKN-C, was built based on the pioneering work of Perkins, Kern, and Nordgren by the combined Carter Equation II for material balance (Howard and Fast, 1957). Without considering fluid leak-off and spurt loss, a 2D fracture model, p-3D models, and 3D models did not clearly illustrate the fracture geometry. Thus, the PKN-C model was suitable to determine the fracture length and width based on the total volume injected during pumping hydraulic fracturing in the Lower Miocene reservoir. The PKN-C model related to the fracture width at the wellbore, fracture half-length, pump rate, flow behavior index, consistency index of the non-Newtonian fluid, and rock properties can be illustrated as (Valko and Economides, 1995):

$$w_i = 9.15^{\frac{1}{2n^2}}\ 3.98^{\frac{n}{2n+2}} \left(\frac{1+2.14n}{n}\right)^{\frac{n}{2n+2}} K^{\frac{1}{2n+2}} \left(\frac{q_i}{2}\right)^n x_f^{\frac{1}{2n+2}} E^{\frac{1}{2n+2}} \tag{1}$$

Based on the Carter II solution (Howard and Fast, 1957) for material balance, which accounted for the leak-off coefficient, spurt loss, and a constant injection rate, the fracture length model can be derived as:

$$x_j = \frac{(w_a+2S_p)\,q_i}{4C_i\pi h_f^2}\left[\exp(\beta^2)\,\mathrm{erfc}(\beta) + \frac{2\beta}{\sqrt{\pi}} - 1\right];\ \beta = \frac{2C_1\sqrt{\pi t_i}}{w_a+2S_p} \tag{2}$$

3. FLUID VISCOSITY AND RHEOLOGY

Fluid selection is currently based on experimentally generated data (Cohen *et al*., 2013) and should minimize formation damage for fractured wells. Fluid viscosity is significantly affected by either the net pressure or the fracture geometries (i.e., fracture width, half-length, and height) and fluid efficiency. It is also influenced by either proppant transport or proppant settling, in which the proppant fall rate did not exceed 10 ft/hr (Jiang *et al*., 2003) based on calculation through the Stokes law model (Smith, 1997), and the fluid properties controlled the leak-off coefficient (wall-building effect). Fluid without the proppant in the pad volume was initially used to create a fracture where the bottom hole treating pressure overcomes the least principal stress of the in-situ stress (Hubbert and Willis, 1957). Due to the downhole high temperature of approximately 149°C, the lithology properties of the Miocene formation were, therefore, the fluid LF-2500 (Schlumberger, 2009) was used for hydraulic fracturing. Most fracturing fluids are non-Newtonian and are commonly used to describe the rheological behavior of fracturing fluid. Therefore, the relationship between the power law parameters, such as flow behavior index, consistency index, and apparent viscosity, is presented in (Smith, 1997) and (Rahim and Holditch, 2003):

$$K = \frac{\mu_a (SR)^{1-n}}{47{,}880} \tag{3}$$

Based on the optimum injection rate for hydraulic fracturing, the shear rate within the fractures near the wellbore can be determined through a specific model (Rahim and Holditch, 2003). Due to the shear rate at the fracture tip reaching zero, the shear rate was calculated based on the average of this value and the shear rate at the fracture tip. The optimum shear rate at 170 sec^{-1} could be obtained based on the optimization tool as:

$$SR = \frac{40.46\, q_i}{2w_i^2 h_f} \tag{4}$$

Where SR is the shear rate in sec^{-1}, q_i is the pump rate in bpm, w_f is the average fracture width in, and h_f is the fracture height in ft at the end of the job. In the field, the fluid viscosity varied, ranging between 40 cP and 500 cP.

4. PUMP RATE

To select the proper pump rate for hydraulic fracturing, which is influenced by the growth of fracture geometries, net pressure, and slurry efficiency, the rate was increased while the fluid efficiency was decreased, and the pump rate decreased as fluid efficiency increased. The pump rate affected the bottom hole treating pressure during pumping. A high rate will cause high bottom hole pressure and requires a higher critical strength of tubing that can lead to tubing failure. The pump rate may also be significantly affected by economic treatment costs. For example, the pump rate increases as the pump horsepower increases, and the pump rate decreases as the pump horsepower decreases. The slurry efficiency was defined as the ratio of the volume the hydraulic fracture created (V_f) to the volume of the injected fracturing fluid (V_i) (Bair, Freeman, and Senko, 2010). The fluid efficiency ensures that it must be maintained between 0.5 and 1 (Smith, 1997).

$$\eta = \frac{V_f}{V_i};\ HP = \frac{q\,\Delta P}{40.8} \quad (5)$$

Where q is the pump rate of hydraulic fracturing in bpm, and Δp is the surface treating pressure in psi. Thus, the slurry efficiency changed as a function of the volume of the injected fracturing fluid, the volume of fluid lost through the fracture area, and the volume of the created fracture. The slurry efficiency depends on the characteristic formation of the fluid leak-off, permeability and porosity of the formation, characteristic fracturing fluid, and the fluid additive. In the field, the injection rate was considered to vary between 16 and 30 bpm.

5. PUMP SCHEDULE

Hydraulic fracturing involves various stages, such as the pad stage, slurry stage, and flush stage, each of which has specific tasks. Moreover, the pad stage involves injecting pressurized fracturing fluid without proppant, and it is initiated to create and propagate fractures. The pad volume without proppant of the total fluid volume injected was the first stage in which a fracture was initially created before the proppant distribution was placed within the fracture. The second stage was a proppant slurry volume injected into the rock formation, where the proppant was added to the fracturing fluid to increase the proppant concentration until the end of the job. This stage played an essential role in maintaining the fracture open as it prevents fracture closure and maintains fracture conductivity. The proppant loading at the end of the job depended on the proppant transporting abilities through the fracturing fluid properties and the capacity of the reservoir that was created by the fracture volume. Per the selected pumping schedule, hydraulic fracturing was considered uniform in the proppant distribution level inside the fractures, and at the end of the job, to increase the fracture conductivity and productivity (Yang *et al*., 2017). The conductivity depends on several parameters such as proppant placement, closure pressure, proppant damage factor, and proppant flow back after shut-in. However, the major influence on fracture conductivity is how to transport proppant slurry from the surface to the fractures, as well as high uniform proppant concentration in the fractures to reach 2 lb/ft² (Smith, 1997). During pumping, as the fracture grows at any time, the general material balance is presented as if $V_i = V_f + V_L$. Here, V_i is the total injection volume injected (qti), which includes the proppant volume, V_f is the fracture volume created, and V_L is the fluid volume leaked through the fracture surface area. The fracture area, A_f, is $4x_fh_f$, and the fracture volume, V_f, at any time for the linear fracture propagation follows the PKN fracture model, and is calculated from the two wings of fractures (Economides and Nolte, 1989):

$$V_f = \frac{\pi \gamma x_f h_f w_f}{2} \quad (6)$$

The propped width after closure pressure of fracture (Economides *et al*., 1994):

$$w_p = \frac{W_{pr}}{2x_f h_f (1-\Phi_p)\rho_p} \quad (7)$$

Here, W_{pr} is the proppant usage that is injected into the fractures, $2x_fh_f$ is the propped fracture area of two fracture wings, and it is assumed that the mass of proppant has been injected into the fractures as it is placed uniformly in the fracture. The relationship between the total volume injected (V_i) and the pad volume (V_{pad}) is based on the slurry efficiency (η) (Nolte 1986; Meng and Brown, 1987).

$$V_{pad} = \frac{V_i(1-\eta)}{1+\eta} \quad (8)$$

The proppant usage to be injected can be calculated from the following model (Rahman *et al*., 2003b)

$$W_{pr} = \frac{V_{pl}}{\frac{1}{\overline{P_c}}+\frac{1}{\rho_p}} \quad (9)$$

Where; $\overline{P_c}$ is the average proppant distribution ($\eta\overline{P_c}$) and P_c is the EOJ proppant concentration. The proppant slurry, V_{pl}, which is the total of proppant volume (V_{pr}) and fracturing fluid volume (V_{fl}) is

$$V_{pl} = V_i - V_{pad} \quad (10)$$

Thus, the total volume injected is calculated as

$$V_i = V_{pad} + V_{fl} + V_{pr} \quad (11)$$

The total fracturing fluid volume without proppant, V_{tfl}, is calculated as

$$V_{tfl} = V_{pad} + V_{fl} \quad (12)$$

The fracturing fluid volume, V_{fl}, is used to mix with dry proppant is given by:

$$V_{fl} = \frac{W_{pr}}{\overline{P_c}} \quad (12)$$

To design the pump schedule, fluid efficiency was a crucial factor for determining the number of stages of hydraulic fracturing based on 2D fracture models (i.e., Radial, PKN, GDK). Based on a material balance, the proppant added concentration, as a ramped proppant schedule with time, is described in the equation below (Nolte, 1986):

$$C_p(t) = C_f\left(\frac{t-t_{pad}}{t_i-t_{pad}}\right)^{\frac{1-\eta}{1+\eta}} \quad (13)$$

Where $C_p(t)$ is the proppant concentration at time t, t_{pad} is the time to pump pad volume, t_i is the total time, and C_f is the proppant added concentration at the end of the job (ppg). In this work, the proppant loading at the end of the job varied between 7 ppg and 10 ppg. To design the flush volume of the hydraulic fracturing, it should be designed to displace the volume of the proppant slurry from the wellbore into the fracture. Moreover, it should be less than the wellbore volume, as the overall displacement may cause proppant flow back to the surface and will result in a choked fracture after dissipating hydraulic fracturing and fracture closure. The flush volume is considered a fluid type: linear gel with a guar concentration of 25 pptg.

6. OPTIMIZATION TECHNIQUES

The design of the experimental method consists of modeling the full factorial, partial factorial, and central composite rotatable design. One of the efficient alternative designs of experiment was the central composite face design with one-half fraction of a 2^k factorial design, 2^{k-1}. Its design is a 2^{k-1} fractional factorial. The central composite face design is commonly used for fitting second-order models. The total number of runs for CCFD is $2^{k-1} + 2k + n_0$, including one-half of the fraction of the standard 2^k factorial points, 2k points fixed axially at a distance, and n_0, which replicates the tests at the center, and k is the variable. Response surface methodology is a mathematical and statistical method to determine the design factor settings based on the multivariate nonlinear model, which has been widely used to optimize the variables of the process. Response surface methodology combines the design of experiments to provide a reliable measurement of response. The mathematical model is the correlation between several variables and one or more responses by fitting the model obtained from the experimental design and determining the optimization values of the independent variables that provide the maximum or minimum response (Cornell 1990; Montgomery 2001; Myers and Montgomery 2002; Myers et al. 2008). By using RSM, a quadratic polynomial equation was built to relate the response as a function of the independent variables and interactional variables (Box and Draper 1987). The response of a quadratic polynomial is described as:

$$Y = \beta_0 + \sum\beta_i X_i + \sum\beta_{ii} X_i^2 + \sum\beta_{ij} X_i X_j + \varepsilon \tag{14}$$

Where Y is the predicted response, β_0 is the intercept, β_i are the linear coefficients, β_{ii} are the interaction coefficients, and X_i and X_j are the independent variables, which are both coded variables. In this study, the second-order polynomial equation was determined based on the un-coded independent variables:

$$\begin{aligned} \mathrm{Y} = \ & \beta_0 + \beta_1 X_1 + \beta_2 X_2 + \beta_3 X_3 + \beta_4 X_4 + \beta_5 X_5 + \beta_6 X_6 \\ & + \beta_{11} X_1^2 + \beta_{22} X_2^2 + \beta_{33} X_3^2 + \beta_{44} X_4^2 + \beta_{55} X_5^2 + \beta_{66} X_6^2 \\ & + \beta_{12} X_1 X_2 + \beta_{13} X_1 X_3 + \beta_{14} X_1 X_4 + \beta_{15} X_1 X_5 + \beta_{16} X_1 X_6 \\ & + \beta_{23} X_2 X_3 + \beta_{24} X_2 X_4 + \beta_{25} X_2 X_5 + \beta_{26} X_2 X_6 \\ & + \beta_{34} X_3 X_4 + \beta_{35} X_3 X_5 + \beta_{36} X_3 X_6 \\ & + \beta_{45} X_4 X_5 + \beta_{46} X_4 X_6 + \beta_{56} X_5 X_6 \end{aligned} \tag{15}$$

7. EXPERIMENTAL DESIGN FOR VARIABLES OF HYDRAULIC FRACTURING

The free design variables in this study included the fracturing fluid viscosity, μ (cP), leak-off coefficient, C_l (ft/min$^{0.5}$), total pumping time, t_i (minutes), injection rate, q (bpm), and the proppant at the end of the job, P_c (ppg), and the ratio of the fracture height migration to the pay zone height, (h_f/h). Ideally, the first five variables are designed on the surface, as those variables can be changed if the parameters achieve optimal fracture treatment performance of the fractured well based on either the maximum fracture length or high fracture conductivity. From the field, the design parameters on the surface and fracture height migration range within the lower and upper bounds are as follows:

16 bpm ≤ q_i ≤ 30 bpm: field experience
60 minutes ≤ t_i ≤ 90 minutes: field experience
7 ppg ≤ P_c ≤ 10 ppg: industry practice (Meng and Brown, 1987)
0.0027 ft/min$^{0.5}$ ≤ C_l ≤ 0.007 ft/min$^{0.5}$: field experience
40 cP ≤ μ ≤ 500 cP: field experience
1 ≤ h_f/h ≤ 2: (M.M. Rahman *et al*., 2003)

The number of tests for the central composite face design with the center point of three based on one-half fraction of the standard 2k factorial points for six variables was $2^{6-1} + 2\times6 + 3 = 47$. The six independent variables and their levels for CCFD used in this research are shown in Table-1. Using the relation of variable levels in Table-1, the coded variables and the actual variables for each design matrix were determined as given in Table-2. Based on Table-2, these experiments were conducted to obtain the response. Two-dimensional fracture models (PKN-C) accounted for the fluid leak-off coefficient, which was used to predict the fracture length of hydraulic fracturing for the Miocene reservoir. The Mfrac simulation may assist in determining the fracture length of each experimental design under the injected volume and pump schedule presented in Table-1.

VOL. 21, NO. 8, APRIL 2026 ISSN 1819-6608
ARPN Journal of Engineering and Applied Sciences

www.arpnjournals.com

Table-1. Reservoir and well data.

Parameters	Values	Parameters	Values
Reservoir drainage area	164 acres	Total system compressibility	1.45×10^{-5} psi^{-1}
Reservoir depth	812 ft	Minimum horizontal stress	5755 psi
Reservoir thickness	85.3 ft	Maximum horizontal stress	6820 psi
Reservoir porosity	13.5%	Vertical stress	7185 psi
Reservoir permeability	2.7 mD	Young's modulus	3×10^{6} psi
Reservoir temperature	215°F	Poisson's ratio	0.27
Reservoir temperature	221°F	Wellbore radius	0.25 ft
Oil saturation	83%	Formation volume factor	1.4 bbl/bbl
Gas saturation	17%	Fracture fluid viscosity	1.4 cP
Fracture toughness	1099 psi $in^{0.5}$	Tubing inside diameter	2.992 in
Density of fracturing fluid	8.5 lb/gal	Tubing outside diameter	3.5 in
Treating fluid type (3-5% KCl brine)			

Table-2. Proppant selection data.

Parameters	Values
Proppant type	16/30 Sintered Ball Bauxite
Specific gravity	3.65
Strength	High strength proppant
Average diameter	0.038 in
Proppant pack porosity	0.35
Conductivity @ closure pressure (at 2 lb/ft²)	11,664 mD.ft
Conductivity damage factor	0.5

Table-3. Six variables and their levels for CCFD.

Variable	Symbol	Coded variable Low (-1)	Center (0)	High (1)
P_c, ppg	X_1	7	8.5	10
Fluid viscosity, cP	X_2	40	270	500
Injection rate, q, bpm	X_3	16	23	30
Injection time, t_i minutes	X_4	60	75	90
Leak-off coefficient, C_l, $ft/min^{0.5}$	X_5	0.00227	0.004635	0.007
h_f/h	X_6	1	1.5	2

VOL. 21, NO. 8, APRIL 2026 ISSN 1819-6608
ARPN Journal of Engineering and Applied Sciences

Table-4. The Central composite design with six independent variables.

Run	Coded level of the variables						Actual level of the variables						Response (Observed)	
	X1	X2	X3	X4	X5	X6	Pc, ppg	Fluid viscosity, cP	Injection rate, q, bpm	Injection time, t_i, minutes	Leak-off coefficient, C_l, ft/min$^{0.5}$	h_f/h	Fracture length, ft	Fracture width, in
1	-1	-1	-1	-1	-1	-1	7	40	16	60	0.00227	1	349.4	0.197
2	1	-1	-1	-1	-1	1	10	40	16	60	0.00227	2	307.2	0.196
3	-1	1	-1	-1	-1	1	7	500	16	60	0.00227	2	258.8	0.344
4	1	1	-1	-1	-1	-1	10	500	16	60	0.00227	1	315.1	0.356
5	-1	-1	1	-1	-1	1	7	40	30	60	0.00227	2	533.9	0.259
6	1	-1	1	-1	-1	-1	10	40	30	60	0.00227	1	626.4	0.264
7	-1	1	1	-1	-1	-1	7	500	30	60	0.00227	1	548.6	0.476
8	1	1	1	-1	-1	1	10	500	30	60	0.00227	2	433	0.455
9	-1	-1	-1	1	-1	1	7	40	16	90	0.00227	2	339.2	0.348
10	1	-1	-1	1	-1	-1	10	40	16	90	0.00227	1	402.2	0.357
11	-1	1	-1	1	-1	-1	7	500	16	90	0.00227	1	398.1	0.376
12	1	1	-1	1	-1	1	10	500	16	90	0.00227	2	333.6	0.366
13	-1	-1	1	1	-1	-1	7	40	30	90	0.00227	1	786.2	0.279
14	1	-1	1	1	-1	1	10	40	30	90	0.00227	2	682.1	0.274
15	-1	1	1	1	-1	1	7	500	30	90	0.00227	2	563.3	0.485
16	1	1	1	1	-1	-1	10	500	30	90	0.00227	1	698.7	0.505
17	-1	-1	-1	-1	1	1	7	40	16	60	0.007	2	121	0.157
18	1	-1	-1	-1	1	-1	10	40	16	60	0.007	1	125.7	0.154
19	-1	1	-1	-1	1	-1	7	500	16	60	0.007	1	122.1	0.281
20	1	1	-1	-1	1	1	10	500	16	60	0.007	2	114.5	0.28
21	-1	-1	1	-1	1	-1	7	40	30	60	0.007	1	232.7	0.207
22	1	-1	1	-1	1	1	10	40	30	60	0.007	2	221.6	0.209
23	-1	1	1	-1	1	1	7	500	30	60	0.007	2	205.9	0.376
24	1	1	1	-1	1	-1	10	500	30	60	0.007	1	223.8	0.38
25	-1	-1	-1	1	1	-1	7	40	16	90	0.007	1	154.7	0.162
26	1	-1	-1	1	1	1	10	40	16	90	0.007	2	149.8	0.165
27	-1	1	-1	1	1	1	7	500	16	90	0.007	2	142.7	0.295
28	1	1	-1	1	1	-1	10	500	16	90	0.007	1	150.9	0.295
29	-1	-1	1	1	1	1	7	40	30	90	0.007	2	275.1	0.22
30	1	-1	1	1	1	-1	10	40	30	90	0.007	1	287	0.218
31	-1	1	1	1	1	-1	7	500	30	90	0.007	1	277.4	0.4
32	1	1	1	1	1	1	10	500	30	90	0.007	2	258	0.397
33	-1	0	0	0	0	0	7	270	23	75	0.004635	1.5	272.3	0.324
34	1	0	0	0	0	0	10	270	23	75	0.004635	1.5	272.3	0.324
35	0	-1	0	0	0	0	8.5	40	23	75	0.004635	1.5	286.9	0.207
36	0	1	0	0	0	0	8.5	500	23	75	0.004635	1.5	266.3	0.374
37	0	0	-1	0	0	0	8.5	270	16	75	0.004635	1.5	193.7	0.273
38	0	0	1	0	0	0	8.5	270	30	75	0.004635	1.5	348.5	0.366
39	0	0	0	-1	0	0	8.5	270	23	60	0.004635	1.5	240.6	0.314
40	0	0	0	1	0	0	8.5	270	23	90	0.004635	1.5	301.1	0.331
41	0	0	0	0	-1	0	8.5	270	23	75	0.00227	1.5	1016.3	0.458
42	0	0	0	0	1	0	8.5	270	23	75	0.007	1.5	191	0.296
43	0	0	0	0	0	-1	8.5	270	23	75	0.004635	1	285.8	0.325
44	0	0	0	0	0	1	8.5	270	23	75	0.004635	2	259.9	0.322
45	0	0	0	0	0	0	8.5	270	23	75	0.004635	1.5	272.5	0.324
46	0	0	0	0	0	0	8.5	270	23	75	0.004635	1.5	272.5	0.324
47	0	0	0	0	0	0	8.5	270	23	75	0.004635	1.5	272.5	0.324

The fracture length and maximum fracture width near the wellbore were presented as the responding independent variables found in the experimental design matrix. The sequence of each experimental data point was used for validating the single response model of the

VOL. 21, NO. 8, APRIL 2026 ISSN 1819-6608
ARPN Journal of Engineering and Applied Sciences

www.arpnjournals.com

operation process. The experiment was randomized to minimize the effects of the uncontrolled factors.

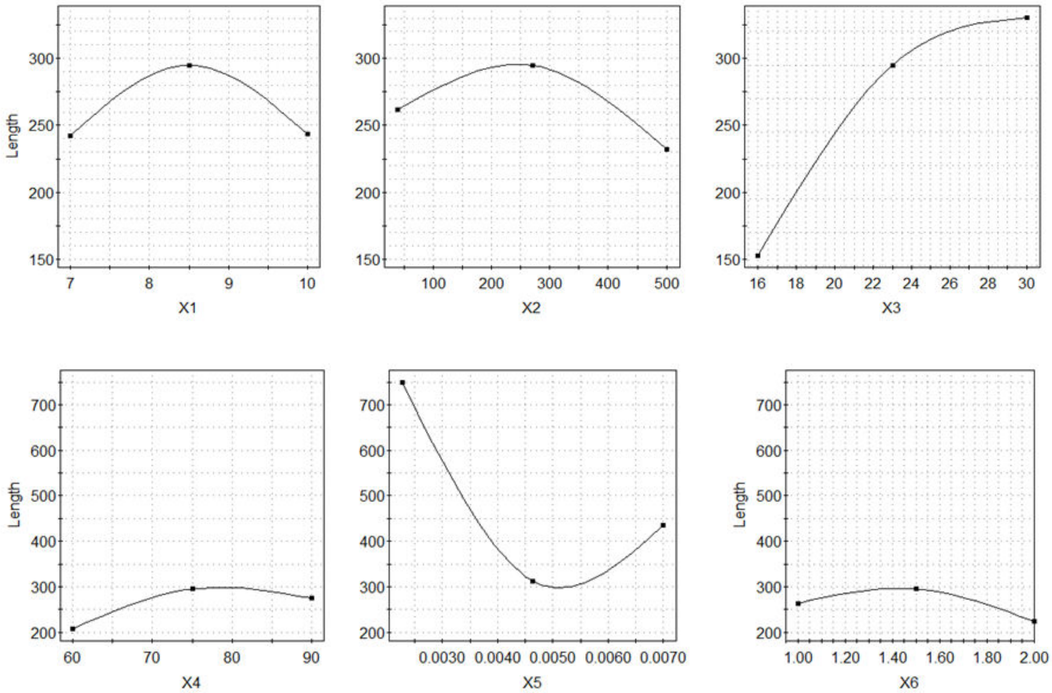

Figure-1. Effects of variables on the fracture length.

Table-5. ANOVA for response surface quadratic model.

Length, ft	DF	SS	MS	F	P	SD
Total	47	6.68E+06	142121			
Constant	1	5.04E+06	5.04E+06			
Total Corrected	46	1.64E+06	35645.8			188.801
Regression	27	1.49E+06	55092.2	6.87661	0	234.717
Residual	19	152219	8011.53			89.5072
N = 47	Q^2 = 0.58		RSD = 89.5072			
DF = 19	R^2 =0.907		$R^2_{Adj.}$ =0.775			

VOL. 21, NO. 8, APRIL 2026 ISSN 1819-6608
ARPN Journal of Engineering and Applied Sciences

www.arpnjournals.com

Table-6. Regression coefficients of the predicted quadratic polynomial model.

No	Length	Coeff. SC	Std. Err.	P
1	Constant	312.447	26.6889	3.93E-10
2	X1	0.602937	15.3504	0.96908
3	X2	-16.7735	15.3504	0.288182
4	X3	94.8088	15.3504	6.19E-06
5	X4	35.8765	15.3504	0.030529
6	X5	-157.006	15.3504	3.65E-09
7	X6	-23.0941	15.3504	0.148903
8	X1*X1	-52.1315	58.025	0.3802
9	X2*X2	-47.8315	58.025	0.419983
10	X3*X3	-53.3315	58.025	0.369559
11	X4*X4	-53.5815	58.025	0.367367
12	X5*X5	279.219	58.025	0.000121
13	X6*X6	-51.5816	58.025	0.385145
14	X1*X2	0.02811	15.8228	0.998549
15	X1*X3	-0.1719	15.8228	0.991454
16	X1*X4	0.959365	15.8228	0.952282
17	X1*X5	-0.65937	15.8228	0.967198
18	X1*X6	3.10313	15.8228	0.8466
19	X2*X3	-10.0906	15.8228	0.531262
20	X2*X4	1.32811	15.8228	0.933984
21	X2*X5	12.6594	15.8228	0.433559
22	X2*X6	-2.82813	15.8228	0.860037
23	X3*X4	13.8906	15.8228	0.390972
24	X3*X5	-39.6406	15.8228	0.021499
25	X3*X6	-8.01563	15.8228	0.618272
26	X4*X5	-15.7094	15.8228	0.333269
27	X4*X6	-1.98438	15.8228	0.901514
28	X5*X6	18.3719	15.8228	0.259981

8. RESULTS AND DISCUSSION

The response surface is statistical and mathematical and optimizes parameters, which is more advantageous than single parameter optimization. This method can save time through the raw material injection of hydraulic fracturing. There was a total of 47 cases with six independent variables from CCFD for optimizing the individual parameter. Table-4 shows the matrix design and results of the fracture length according to the design of the experiment. The maximum fracture length was obtained at 1016.3 ft in run 41 under operating conditions of the proppant concentration of 8.5 ppg, fluid viscosity of 270 cP, an injection rate of 23 bpm, an injection time of 75 minutes, and a fracture height migration to the pay zone height ratio of 1.5. In addition, the maximum fracture width at the near wellbore is collected from run 16. By using the response surface method with the observed data, the correlation between the response of the fracture length and the variables and the interaction variables under the coded variables was presented by following the second-order polynomial equation.

VOL. 21, NO. 8, APRIL 2026 ISSN 1819-6608
ARPN Journal of Engineering and Applied Sciences

www.arpnjournals.com

$$\begin{aligned}
Y = \; & 312.447 + 0.602937X_1 - 16.7735X_2 + 94.8088X_3 + 35.8765X_4 \\
& -157.006X_5 - 23.0941X_6 \\
& -52.1315X_1^2 - 47.8315X_2^2 - 53.3315X_3^2 - 53.5815X_4^2 \\
& +279.219X_5^2 - 51.5816X_6^2 \\
& +0.0281103X_1X_2 - 0.171895X_1X_3 + 0.959365X_1X_4 \\
& -0.659368X_1X_5 + 3.10313X_1X_6 \\
& -10.0906X_2X_3 + 1.32811X_2X_4 + 12.6594X_2X_5 \\
& -2.82813X_2X_6 + 13.8906X_3X_4 - 39.6406X_3X_5 \\
& -8.01563X_3X_6 - 15.7094X_4X_5 - 1.98438X_4X_6 \\
& +18.3719X_5X_6
\end{aligned} \tag{16}$$

The coefficient of determination (R^2=0.907) was shown through an analysis of variance of the quadratic regression model, which proved that a lesser percentage of the total variation was not explained by the model. The model demonstrated that it was highly significant.

8.1 The Main and Interaction Effect Plots

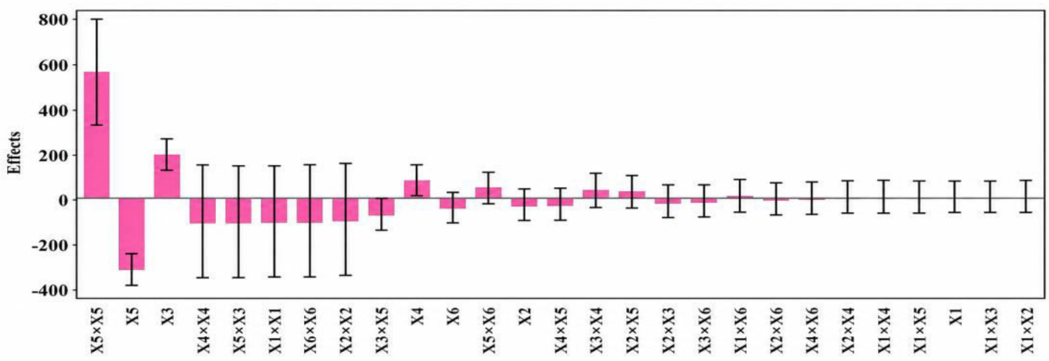

Figure-2. The coefficient factors affect the fracture length.

Figure-2 presents the effect plot of the variables on the fracture length. This graph can be separated into two areas. The first area is shown to be below zero in which the coefficient factors of the independent variables, and the interaction variables illustrated negative coefficients, including X2, X5, X6, X1.X1, X2.X2, X3.X3, X4.X4, X6.X6, X1.X3, X1.X5, X2.X3, X2.X6, X3.X5, X3.X6, X4.X5, and X4.X6, which decreased the fractured length. X6 is presented as the fracture height migration compared with the pay zone height, where the coefficient factor of the independent variable is below zero. The importance of the coefficient factor of the fracture height migration to the boundary layers was not economical for many fields, and previous research has shown that these layers do not improve oil production. In this research, the constrained fracture height was not to increase in the bounding layers by more than 25% of the pay zone height (Smith, 1992). This study obtained the optimization h_f/h of 1.065 (226.2 ft) through the response surface method, where the maximum fracture length was 828 ft. Figure-3 shows the effect of the hf/h on the fracture length, and the h_f/h increased as the fracture length decreased. The bounding layers did not directly produce oil production, but the fracture height migration into the bounding layers may assist in production for two reasons: first, the increase in the fracture height migration to the bounding layers allows for the growth of the fracture width and increases production. Second, the non-producible fracture width around the edges of the bounding layers located in the pay zone layers, which may improve production. However, the excessive fracture height migration to the bounding layers was not beneficial, as it is the treatment cost of hydraulic fracturing (Rahman et al., 2003). The second region was presented as factors above zero, which indicate positive coefficient factors, including X1, X3, X4, X5.X5, X1.X2, X1.X4, X1.X6, X2.X4, X2.X5, X3.X4, and X5.X6, indicating an increase in the fracture length.

8.2 Optimization of Parameters for the Maximum Fracture Length

Three-dimensional surface plots and contour plots were obtained from the full quadratic model of Equation 16 to correlate the relationship between the independent variables and the dependent variables on the fracture length. The graphics represent the response surfaces. The contour plots were determined through the results of the fracture length, which was affected by the proppant concentration at the end of the job, fluid viscosity, injection rate, injection time, the leak-off coefficient, and the fracture height migration to the pay zone height ratio (Figures 3 & 4). In the two figures, the maximum predicted value, as the maximum fracture length, was presented through the surface that contained

VOL. 21, NO. 8, APRIL 2026 ISSN 1819-6608
ARPN Journal of Engineering and Applied Sciences

the smallest ellipse in the contour diagram. The elliptical shape of the contours was clearly closed where there was a complete interaction between the independent variables. The contour plot and the response surface plots showed the maximized fracture length region according to the optimum operating parameters (Figures 3 & 4). In Figure-3, the smallest red ellipse area determined the regional area for maximizing the fracture length. The maximum fracture length reached 828 ft at the operating parameter conditions, such as the proppant concentration at the end of the job of 8.6 ppg, fluid viscosity of 47.8 cP, an injection rate of 30 bpm, an injection time of 79 minutes, the leak-off coefficient of 0.0023 ft/min$^{0.5}$, and a ratio between the fracture height migration and the pay zone height of 1.065. New optimal parameters have been considered and applied for hydraulic fracturing in the Lower Miocene formation. Each parameter from the six independent variables was affected by the fracture length, reflecting the significance of the regression coefficients from the quadratic polynomial model and the gradient of the slope in the response surface plot.

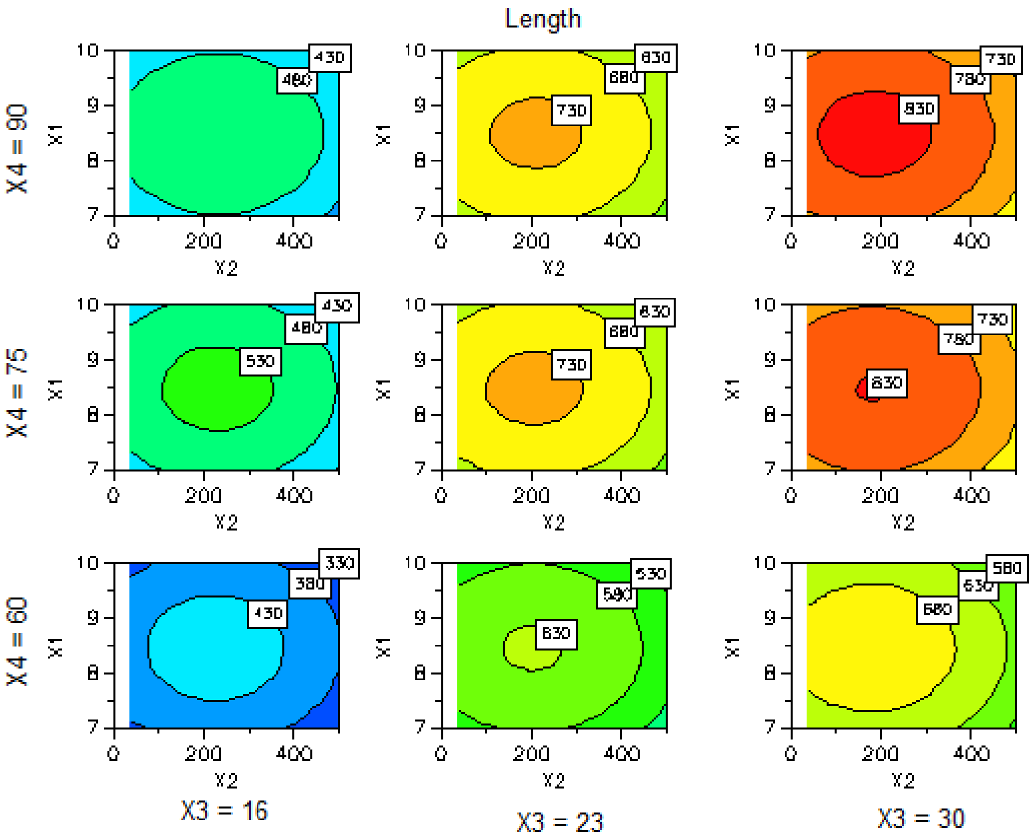

Figure-3. The effects of variables on fracture length are presented by contour plots.

VOL. 21, NO. 8, APRIL 2026 ISSN 1819-6608
ARPN Journal of Engineering and Applied Sciences

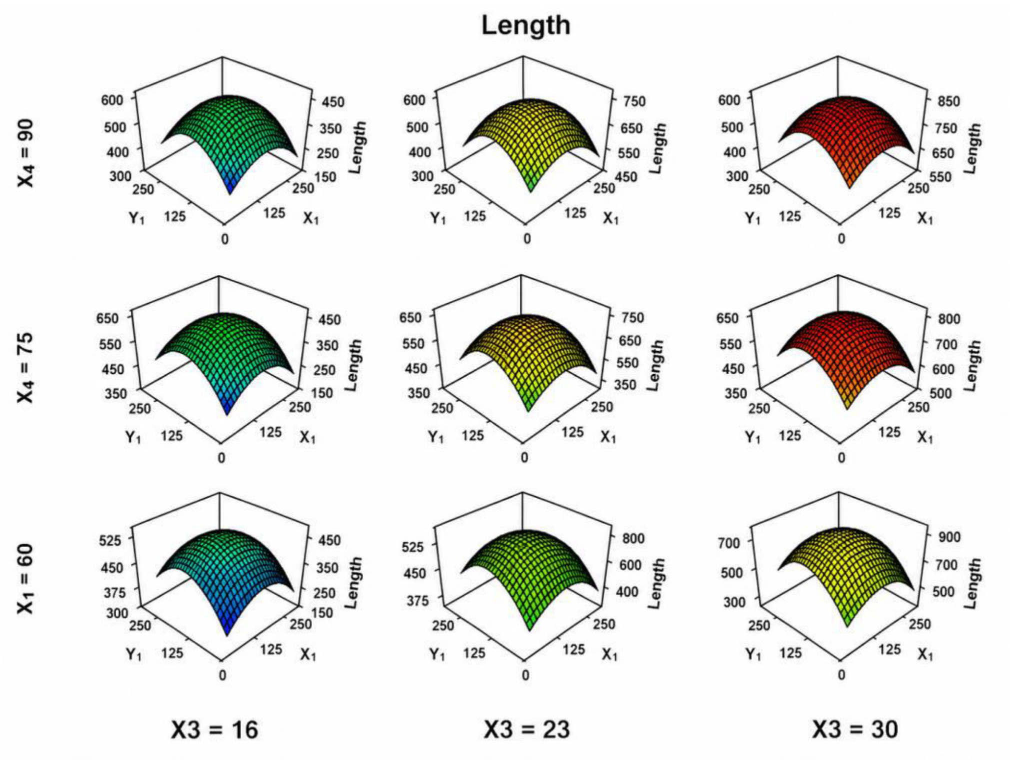

Figure-4. The effects of variables on the fracture length are shown by response surface plots.

Table-7. The results of optimal fracture geometry at the optimal treatment variables.

No	P_c, ppg	μ, cP	q, bpm	t_i, min	C_l, ft/min$^{0.5}$	h_f, ft	x_f, ft	W_a, in	M_p, Proppant mass, lbs
Value	8.6	47.8	30	79	0.0023	129.3	828	0.17	140443

To compare with the optimal result of a fracture length of 828 ft reported in Table-7, the Unified Fracture Design (UFD) is based on a M_p of 140,443 lb, a porosity of 0.30, a density of 227.76 lb/ft³, a net pay height of 121.4 ft, a reservoir permeability of 0.5 mD, a fracture permeability of 80,000 mD, and a drainage radius of 1640 ft. The optimized UFD results yield a dimensionless proppant number of 0.275 and an optimal fracture conductivity of 1.64, corresponding to a fracture length of approximately 823 ft and an average fracture width of 0.105 in.

9. OPTIMIZATION OF THE FRACTURE WIDTH

Table-8. ANOVA for response surface quadratic model.

Fracture width, in	DF	SS	MS	F	P	SD
Total	47	4.91005	0.104469			
Constant	1	4.54704	4.54704			
Total Corrected	46	0.363008	0.007891			0.0088339
Regression	27	0.348564	0.012909	16.918	0.000	0.113621
Residual	19	0.014444	0.000760			0.027579
N = 47		$Q^2 = 0.670$	RSD = 0.0276			
DF = 19		$R^2 = 0.960$	$R^2adj = 0.904$			

ISSN 1819-6608
ARPN Journal of Engineering and Applied Sciences

Table-9. Regression coefficients of the predicted quadratic polynomial model.

Width, in	Term	Coeff. SC	Std. Err.	P-value
1	Constant	0.328701	0.008221	8.38E-02
2	X_1	0.000248	0.004729	0.958733
3	X_2	0.075604	0.004729	1.78E-12
4	X_3	0.034458	0.004729	6.51E-07
5	X_4	0.011683	0.004729	0.002247
6	X_5	-0.04421	0.004729	1.54E-08
7	X_6	-0.00253	0.004729	0.599541
8	X_1*X_1	-0.00666	0.017874	0.713403
9	X_2*X_2	-0.0398	0.017874	0.038266
10	X_3*X_3	-0.01049	0.017874	0.564228
11	X_4*X_4	-0.00744	0.017874	0.681735
12	X_5*X_5	0.046716	0.017874	0.017081
13	X_6*X_6	-0.00673	0.017874	0.710353
14	X_1*X_2	-0.00026	0.004874	0.958168
15	X_1*X_3	-0.00026	0.004874	0.957766
16	X_1*X_4	0.000503	0.004874	0.918916
17	X_1*X_5	-0.00025	0.004874	0.958865
18	X_1*X_6	-0.00914	0.004874	0.076222
19	X_2*X_3	0.0214	0.004874	0.000314
20	X_2*X_4	-0.00649	0.004874	0.198623
21	X_2*X_5	0.000784	0.004874	0.873901
22	X_2*X_6	-0.00177	0.004874	0.719865
23	X_3*X_4	-0.00775	0.004874	0.128195
24	X_3*X_5	0.004933	0.004874	0.324169
25	X_3*X_6	-0.00081	0.004874	0.870113
26	X_4*X_5	-0.01044	0.004874	0.045433
27	X_4*X_6	-0.00015	0.004874	0.976524
28	X_5*X_6	0.002727	0.004874	0.582337

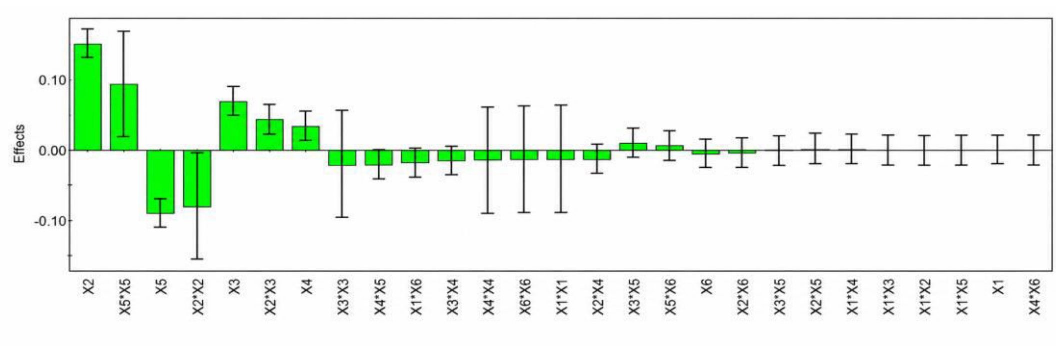

Figure-5. Effects of the coefficient terms on fracture width.

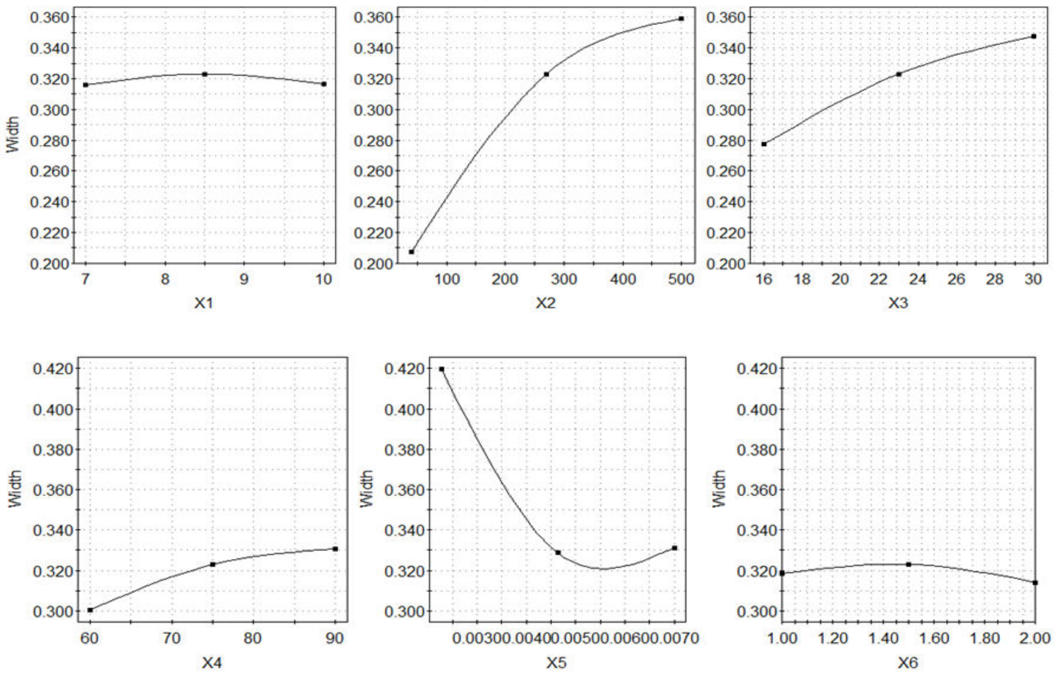

Figure-6. Effects of variables on the fracture width.

Table-4 describes the matrix design and results of the fracture width based on the experimental design and simulation of hydraulic fracturing by Mfrac. Notably, the maximum fracture width was identified at 0.505 in in run 16 of the matrix design under variables of the proppant concentration of 10 ppg, fluid viscosity of 500 cP, an injection rate of 30 bpm, an injection time of 90 minutes, the leak-off coefficient of 0.00227 ft/min$^{0.5,}$ and the fracture height migration to the pay zone height ratio of 1. By using the response surface methodology, the maximum predicted fracture width is contained within the smallest ellipse area of the contour diagram in Figure-7. The contour plot and response surface have been shown in the regional area for optimization of the fracture width. The optimal fracture width is identified as 0.5017 inch under the proppant concentration at the end of the job of 8.8 ppg, fluid viscosity of 483 cP, an injection rate of 29 bpm, an injection time of 87 minutes, the leak-off coefficient of 0.0023 ft/min$^{0.5}$, and the fracture height migration to the pay zone height ratio of 1.2423.

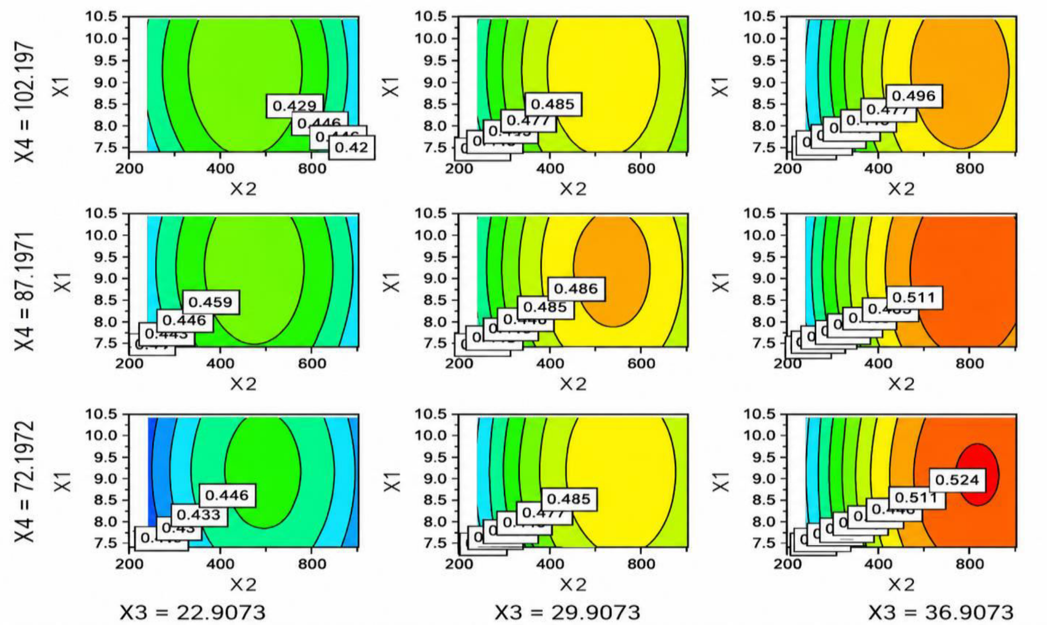

Figure-7. The effects of variables on fracture width are presented by contour plots.

VOL. 21, NO. 8, APRIL 2026 ISSN 1819-6608
ARPN Journal of Engineering and Applied Sciences

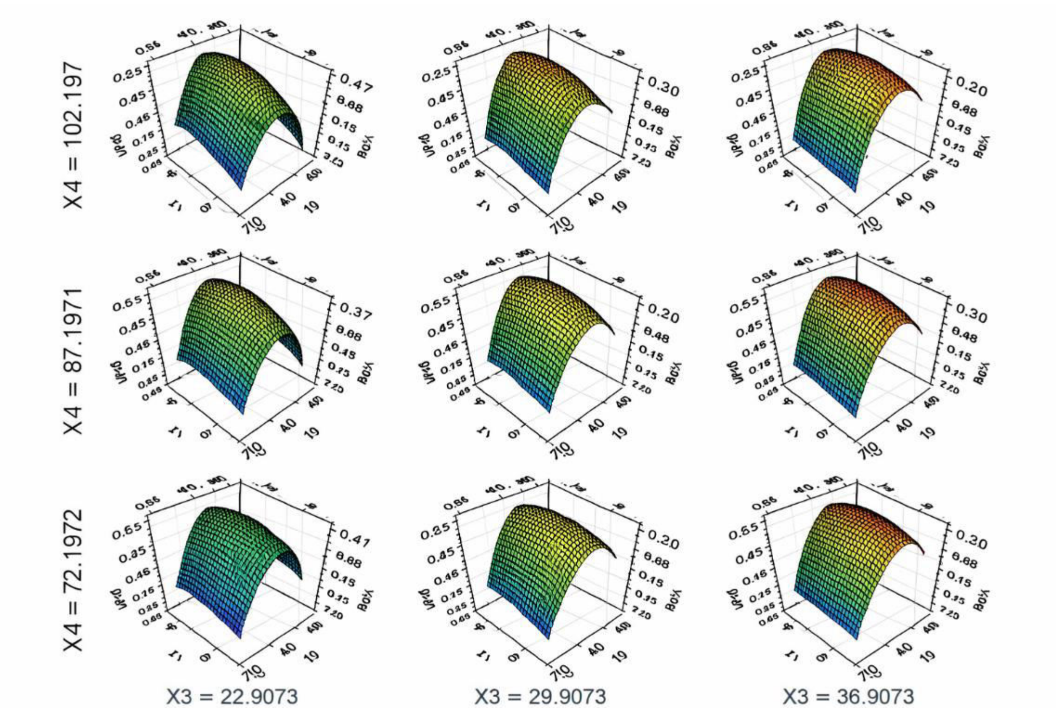

Figure-8. The effects of variables on the fracture width are shown by response surface plots.

10. THE EFFECT OF THE VISCOSITY OF FRACTURING FLUID ON FRACTURE LENGTH

The X_2 variable shown in Figure-1 describes the effect of viscosity on the fracture length for hydraulic fracturing treatment in the Lower Miocene. In this graph, the fluid viscosity design increases between 50 cP and 250 cP as the fracture length significantly increases. This is explained by the fact that sufficient frac fluid viscosity is proportional to the growth of the fracture geometry such as the fracture length, the fracture width, and the net pressure. In addition, the net pressure is proportional to the extension of fracture propagation because the net pressure depends not only on the closure pressure, but also on the frictional systems (i.e., fracturing fluid viscosity, the reservoir height in ft, the density of proppant slurry). In the figure, the fracturing fluid viscosity is increased steadily from 250 cP to 500 cP as the fracture length of hydraulic fracture treatment is decreased, as shown in Figure-2. This is due to the high fracturing fluid viscosity, which increases the frictional systems. It, therefore, decreases the net pressure, reducing the growth of the fracture propagation during hydraulic fracturing.

11. THE EFFECT OF THE FRACTURE HEIGHT MIGRATION ON THE FRACTURE LENGTH

The X_6 shown in Figure-1 presents the effect of fracture height migration to the reservoir height ratio on the fracture length. The fracture length of fracture treatment gradually increases when the fracture height migration to the reservoir height ratio slightly increases between 1 and 1.5. The fracture length reaches a peak, and then it is slightly decreased.

12. CONCLUSIONS

In this paper, an optimization approach has been proposed for improving the design of hydraulic fracture treatment in the Lower Miocene sandstone reservoir. The central composite face design under one-half fraction and response surface methodology with the maximum fracture length objective based on the individual total volume injected and the PKN-C model was considered. The following conclusions can be drawn from this calculation:

- The optimal set of independent variables of hydraulic fracturing for the Lower Miocene sandstone reservoir was obtained for the desired levels of fracture length. The maximum fracture length was determined at 828 ft under the optimum conditions at the proppant concentration at the end of the job of 8.6 ppg, a fracturing fluid viscosity of 47.8 cP, an injection rate of 30 bpm, an injection time of 79 minutes, a leak-off coefficient of 0.0023 ft/min$^{0.5}$, and a fracture-height-migration-to-pay-zone-height ratio of 1.065.

- This study proved that the central composite face design and response surface methodology were successfully applied for the design of hydraulic fracturing of the Lower Miocene sandstone reservoir. This method was optimal for obtaining a maximum fracture length in a short period of time

ARPN Journal of Engineering and Applied Sciences

and had the lowest trial and error for hydraulic fracturing optimization.

ACKNOWLEDGMENTS

This research is funded by Petrovietnam University under the grant code of GV2505

NOMENCLATURE

CCFD	Central Composite Face Design
RSM	Response Surface Methodology
PKN-C	Perkins-Kern-Nordgren with Carter
PKN	Perkins-Kern-Nordgren
KGD	Khristianovitch–Geertsma–de Klerk
NPV	Net Present Value
EOJ	End of Job
ANOVA	Analysis of Variance
SPE	Society of Petroleum Engineers
Mfrac	Mfrac
p-3D	Pseudo-three-dimensional
3D	Three-dimensional
2D	Two-dimensional
Bpm	Barrels per minute
Ppg	Pounds per gallon
cP	Centipoise
pptg	Pounds per thousand gallons
DF	Degrees of Freedom
SS	Sum of Squares
MS	Mean Square
F	F-value
P	P-value
SD	Standard Deviation
R^2	Coefficient of Determination
R^2_{Adj}	Adjusted R^2
Q^2	Predictive relevance
RSD	Residual Standard Deviation
Coeff. SC	Coefficient - Standardized Coefficient
Std. Err.	Standard Error
AIME	American Institute of Mining, Metallurgical, and Petroleum Engineers
API	American Petroleum Institute
ASQC	American Society for Quality Control
EGS	Enhanced Geothermal Systems
LEMIGAS	Lembaga Minyak dan Gas Bumi
NSI	NSI Technologies
LF-2500	Fracturing fluid of Schlumberger
SR	Shear Rate
η	Slurry efficiency

REFERENCES

Aggour T. M. 2001. Optimization strategies for hydraulic fractures in high permeability reservoirs. In SPE Middle East Oil Show. Society of Petroleum Engineers.

Aggour T. M. and Economides M. J. 1998. Optimization of the performance of high-permeability fractured wells. In SPE International Symposium on Formation Damage Control. Society of Petroleum Engineers.

Bair E. S., Freeman D. C. and Senko J. M. 2010. Expert panel technical report: Subsurface gas invasion Bainbridge Township, Geauga County, Ohio. Ohio Department of Natural Resources.

Box G. E. P. and Draper N. R. 1987. Empirical model building and response surfaces. John Wiley & Sons.

Bybee K. 2003. Hydraulic fracturing in the Ghawar field: Carbonate and sandstone reservoirs. Journal of Petroleum Technology, 55(3): 47-48. https://doi.org/10.2118/0303-0047-JPT

Cornell J. A. 1990. How to apply response surface methodology (2nd ed.). American Society for Quality Control.

Cohen A., *et al*. 2013. Optimum fluid and proppant selection for hydraulic fracturing in shale gas reservoirs: A parametric study based on fracturing-to-production simulations (SPE 163876). Society of Petroleum Engineers. https://doi.org/10.2118/163876-MS

Economides M. J., Hill A. D. and Ehlig-Economides C. 1994. Petroleum production systems. Prentice Hall.

Economides M. J., Oligney R. E. & Valko P. P. 2002. Unified fracture design. Orsa Press.

Hoorn K., Heijinen L. J., Gankema M. E. and Nitters G. 2012. Hydraulic fracturing in limestone: A case study of two EGS projects. In Stanford Geothermal Workshop. Stanford University.

Holditch S. A. 1993. Hydraulic fracturing in low permeability reservoirs. Journal of Petroleum Technology.

Howard G. C. and Fast C. R. 1957. Optimum fluid characteristics for fracture extension. American Petroleum Institute.

Hubbert M. K. and Willis D. G. 1957. Mechanics of hydraulic fracturing. Petroleum Transactions, AIME. 210, 153-168.

Jiang T., Wang X. and Shan W. 2003. Hydraulic fracturing technology to minimize formation damage. In SPE European Formation Damage Conference. SPE.

Langedijk R. A., *et al*. 2000. Optimization of hydraulic fracturing in a gas-condensate reservoir. In SPE Annual Technical Conference and Exhibition. SPE.

Meng H. and Brown K. 1987. Coupling of production forecasting and fracture design (SPE 16435). SPE.

Mohaghegh S., Balan B. and Ameri S. 1996. A hybrid neuro-genetic approach to hydraulic fracture design. In SPE Annual Technical Conference and Exhibition. SPE.

Montgomery D. C. 2001. Design and analysis of experiments (5th ed.). John Wiley & Sons.

Myers R. H. and Montgomery D. C. 2002. Response surface methodology (2nd ed.). John Wiley & Sons.

Myers R. H., Montgomery D. C. and Anderson-Cook C. 2008. Response surface methodology (3rd ed.). John Wiley & Sons.

Ngoc T. B. N., Dang T. Q. C., Bae W. and Chung T. 2013. Geological characterization and production optimization in White Tiger field. Journal of Canadian Petroleum Technology.

Nolte K. G. 1986. Determination of proppant and fluid schedules from fracturing pressure decline. SPE Production Engineering.

Perkins T. K. and Kern L. R. 1961. Widths of hydraulic fractures. Journal of Petroleum Technology.

Queipo N. V., Verde A. J., Canelón J. and Pintos S. 2002. Efficient global optimization for hydraulic fracturing design. Journal of Petroleum Science and Engineering. 35, 151-166.

Rachmat R., Pramana A. and Febriana D. 2012. Hydraulic fracturing applications in oil reservoirs. SPE Conference Proceedings.

Rahim Z. and Holditch S. A. 1995. Using 3D concepts in 2D fracture models. Journal of Petroleum Science and Engineering.

Rahim Z. and Holditch S. A. 2003. Modeling shear rate in hydraulic fractures. SPE Production & Operations.

Rahman M. M., Rahman M. K. and Rahman S. S. 2003. Optimizing treatment parameters for enhanced hydrocarbon production. Journal of Canadian Petroleum Technology.

Yang S., Siddhamshetty P. and Kwon S.-I. 2017. Optimal pumping schedule design to achieve a uniform proppant concentration level in hydraulic fracturing. Computers and Chemical Engineering, 113, 66-76. https://doi.org/10.1016/j.compchemeng.2017.09.007

Schlumberger. 2009. Technical proposal: Hydraulic fracturing treatments in White Tiger field. Schlumberger.

Smith M. B. 1997. Hydraulic fracturing (2nd ed.). NSI Technologies.

Priyantoro T. A., Prakoso N. F. and Kahfie R. M. 2012. Journey of hydraulic fracturing improvement to increase oil recovery from sandstone formation in Rimau Block (SPE 156550). Society of Petroleum Engineers. https://doi.org/10.2118/156550-MS

Usman P., Marino D. and Soelistijono M. 2010. Productivity improvement of low permeability gas reservoirs. LEMIGAS Scientific Journal.

Valko P. P. and Economides M. J. 1995. Hydraulic fracture mechanics. John Wiley & Sons.

Zhou Z., Li X., Xu Y., Chong K. K., Marshall E. J. and Zhang B. N. 2006. Multistage hydraulic fracturing in an open-hole ultra-tight sandstone formation in China-Design considerations and execution results (SPE 103671). Society of Petroleum Engineers. https://doi.org/10.2118/103671-MS

Roudakov V. and Rohwer C. 2006. Successful hydraulic fracturing techniques in horizontal wells for sandstone formations in the Permian Basin (SPE 102370). Society of Petroleum Engineers. https://doi.org/10.2118/102370-MS

Zagrebelnyy E., Martynov M. and Konopelko A. 2017. Successful hydraulic fracturing techniques in shallow unconsolidated heavy oil sandstones (SPE 187682). Society of Petroleum Engineers. https://doi.org/10.2118/187682-MS.